Structure of naturally hydrated ferrihydrite revealed through neutron diffraction and first-principles modeling

Helen F. Chappell,[1,2,*] William Thom,[2,3] Daniel T. Bowron,[4] Nuno Faria,[2,3] Philip J. Hasnip,[5] and Jonathan J. Powell[2,3]

[1]*School of Earth and Environment, University of Leeds, Leeds, LS2 9JT, United Kingdom*

[2]*MRC, Elsie Widdowson Laboratory, 120 Fulbourn Road, Cambridge, CB1 9NL, United Kingdom*

[3]*Department of Veterinary Medicine, University of Cambridge, Cambridge, CB3 0ES, United Kingdom*

[4]*ISIS Pulsed Neutron and Muon Source, STFC-Rutherford Appleton Laboratory, Harwell-Oxford, Didcot, OX11 0QX, United Kingdom*

[5]*Department of Physics, University of York, Heslington, York, YO10 5DD, United Kingdom*

(Received 8 June 2017; published 14 August 2017)

Ferrihydrite, with a "two-line" x-ray diffraction pattern (2L-Fh), is the most amorphous of the iron oxides and is ubiquitous in both terrestrial and aquatic environments. It also plays a central role in the regulation and metabolism of iron in bacteria, algae, higher plants, and animals, including humans. In this study, we present a single-phase model for ferrihydrite that unifies existing analytical data while adhering to fundamental chemical principles. The primary particle is small (20–50 Å) and has a dynamic and variably hydrated surface, which negates long-range order; collectively, these features have hampered complete characterization and frustrated our understanding of the mineral's reactivity and chemical/biochemical function. Near and intermediate range neutron diffraction (NIMROD) and first-principles density functional theory (DFT) were employed in this study to generate and interpret high-resolution data of naturally hydrated, synthetic 2L-Fh at standard temperature. The structural optimization overcomes transgressions of coordination chemistry inherent within previously proposed structures, to produce a robust and unambiguous single-phase model.

DOI: 10.1103/PhysRevMaterials.1.036002

I. INTRODUCTION

Ferrihydrite (Fh) is a hydrated iron oxide mineral, ubiquitous in geochemical systems and in biology despite a high solubility product ($\log_{10}{}^{*}K_{SO}$, ~3.96) and tendency towards phase conversion; these factors being outweighed by its rapid formation kinetics. As a consequence of the latter, Fh precipitates readily from aqueous systems across a wide range of pHs (≥2) in preference to slower forming stable minerals such as goethite and hematite. The large specific surface area (>600 m^2/g) of its typical nanocrystalline agglomerates, and associated structural disorder, engender much of Fh's unique chemistry but also hamper characterization. Thus, despite crucial roles in nature [1–3], biology [4], technology [5], and medicine [6], the mineral structure of Fh remains contentious.

Two-line ferrihydrite (2L-Fh), so termed because of the two broad Bragg peaks observed with x-ray diffraction, is the primary natural form of the mineral and has recently been shown to nucleate from a Fe_{13} Keggin ion precursor [7]. With a primary particle size of only 2–5 nm [8] the structural features of 2L-Fh are dominated by surface atoms. This large surface:volume ratio coupled with the consequent loss of long-range order has foiled multiple techniques in the absolute characterization of 2L-Fh particles. Moreover, the mineral surface is dynamic and hydrated, and all attempts to stabilize the core mineral phase through high-temperature treatment have led to surface water loss and inevitable structural changes. For example, Harrington *et al* heated their 2L-Fh samples to 300 °C for 30 minutes under vacuum to increase the crystallinity of the mineral core and remove noise in the neutron diffraction analysis [9]. As a result, structures for 2L-Fh have been proposed from a suite of techniques that have used ferrihydrite in a multitude of different physiochemical forms (Table I).

Notwithstanding, two structures have come to dominate the landscape. The first is the three-component model originally proposed by Drits *et al.* [10]. The model is composed of a defective, randomly occupied phase, a defect-free close packing phase and low levels of ultradispersed hematite [10]. Apart from being the first study to propose a multiphase model, it was also unusual in suggesting that all the Fe would be octahedrally coordinated. In support of this model is the EXAFS and XANES study of Manceau *et al.*, who, in examining the surface structure of Fh, show that the octahedral-only three-phase model provides a match for their experimental data [11]. In contrast, there are numerous studies, from the early EXAFS and x-ray absorption edge spectroscopy of Heald [12] and Eggleton [13] to the electron energy loss spectroscopy study of Vaughan *et al.* in 2012 [14], which show that the mineral contains *both* octahedral and tetrahedral iron sites, although there is disagreement over the actual percentage of tetrahedral Fe. The second predominant structure is a single-phase model, proposed by Michel *et al.* [15,16]. It is based upon isostructural akdalaite and has a lot in common with the earliest structures, with its mix of octahedral and tetrahedral Fe sites [12,13,15], and was determined from XRD generated pair distribution functions (PDFs) [9,15]. In support of this model, there are many studies that conclude the mineral phase must include *both* tetrahedrally and octahedrally coordinated Fe [Table I; [12–15,17,18]]. However, this single-phase model demonstrates certain structural anomalies, e.g., Refs. [19–22], namely, tetrahedral Fe-O bonds, which are effectively too long, giving tetrahedral and octahedral volumes that are equal, and an unrealistically short bond within that

*Correspondence and requests for materials should be to this author.

TABLE I. Landmark studies in the structural analysis of ferrihydrite, illustrating the different types of samples and techniques employed.

Study	Techniques	Sample	Implications
Towe *et al.*, 1967 [23]	IR; XRD; differential thermal analysis	Ferritin; 2L-Fh, prepared at 85 °C. Samples dried at 50 °C and 110 °C	Hematite-like structure; Oct and Tet Fe sites
Harrison *et al.*, 1967 [4]	X-ray and electron diffraction	Ferritin	Oct and Tet Fe sites
Heald *et al.*, 1979 [12]	EXAFS	Ferritin	Oct and Tet Fe sites
Eggleton *et al.*, 1988 [13]	X-ray Absorption Edge Spectroscopy; electron microscopy; X-ray powder diffraction; thermal analysis	2L-Fh and 6L-Fh. Prepared at 60 °C and 75 °C, respectively	Oct and Tet (36%) Fe sites; development of maghemite after 300 °C
Drits *et al.*, 1993 [10]	XRD	2L-Fh and 6L-Fh	Three-component model; defective, defect-free and ultradispersed hematite (10%). Oct Fe only sites
Zhao *et al.*, 1994 [17]	XAFS	2L-Fh and 6L-Fh. Prepared at various temperatures between 50°C−500 °C	Oct and Tet (10%) Fe sites. Tet sites at the surface
Manceau *et al.*, 1997 [11]	XANES	2L-Fh and 6L-Fh prepared at 92 °C and air-dried at 25 °C	Oct Fe sites. Over estimation of Tet Fe sites, from previous study (Zhao *et al.*, Ref. [17])
Jansen *et al.*, 2002 [24]	XRD, Neutron Diffraction	6L-Fh Prepared at 75 °C	No hematite. 50% defective, 50% defect-free phases
Michel *et al.*, 2007 [15]	XRD, PDFs	2L-Fh prepared at 23 °C, 3L-Fh, 6L-Fh prepared at 75 °C	Single-phase model with both Oct and Tet (20%) Fe sites
Rancourt *et al.*, 2008 [19]	XRD	2L-Fh prepared at 60 °C and dried at 110 °C. 6L-Fh prepared at 75 °C	Single-phase structure incorrect
Malliot *et al.*, 2011 [18]	EXAFS	2L-Fh prepared at 75 °C, air-dried. 4L-Fh, 5L-Fh, and 6L-Fh	Oct and Tet (15%–35%)Fe sites
Vaughan *et al.*, 2012 [14]	Electron Energy Loss Spectroscopy	2L-Fh and 6L-Fh. Prepared at 70 °C	Oct and Tet (10%) Fe sites
This Study	Neutron Diffraction, PDFs, XRD, Elemental analysis	2L-Fh, prepared at 20 °C, dried at 40 °C	Single-phase model resolved

same tetrahedral environment, which gives each tetrahedra a large degree of eccentricity, suggesting thermodynamic instability [20].

One recurring issue with all these studies, particularly with the more modern diffraction data, is the lack of analysis on samples without heat-treatment, as only then is surface hydration maintained and the risk of structural changes avoided. Here we used the Near and Intermediate Range Neutron Diffractometer (NIMROD) to generate high-resolution neutron diffraction data of 2L-Fh. The instrument, which is optimized for measuring the diffuse scattering signals of light element containing systems, is ideal for the 2L-Fh nanoparticulate system where there is not well-defined Bragg scattering in the $F(Q)$. This has allowed us to use ferrihydrite dried at just 40 °C, but with no subsequent high-temperature treatment that would risk significant dehydration or even phase change. We have revisited the previous single-phase model of Michel *et al.* and optimized the structure from first principles. Importantly, we have shown that an improved single-phase model, which has all the chemical ambiguities removed, is an excellent match for the experimental data without the need for resorting to overfitted multiphase structures.

II. METHODS

A. Synthesis of ferrihydrite

Two-line ferrihydrite (Fh) was prepared by precipitation-titration; 40-mM ferric chloride solution was neutralized via dropwise addition of 5 M NaOH (at STP) under constant agitation. Precipitates were filtered and washed twice with UHP H_2O, yielding 3.89 g of solid product. Drying to a constant mass at 40 °C yielded 2.16 g of the final product.

B. X-ray diffraction

X-ray diffraction data were collected with a Bruker D8 Power Diffractometer using Cu $K_{\alpha 1}$ radiation, a Ge primary monochromator and a Lynx Eye Detector. The scanning range was $2\theta = 5°$–$70°$ at a speed of 7.5 s/step and a step size of 0.01 degrees.BRUKER EVA software was used to process the data with calibration peaks fitted to references in the ICDD (international center for diffraction data) database.

C. Elemental analysis

The total iron content was determined after acid dissolution by inductively coupled plasma optical emission spectrometry

TABLE II. Relative (to Fe) elemental abundances of synthesized two-line ferrihydrite. The mineral is principally composed of iron, oxygen, and hydrogen—quantified by inductively coupled plasma optical emission spectrometry (ICP-OES), Unterzaucher pyrolysis and Dumas combustion, respectively. Trace levels of carbon and chlorine arising from the mineral synthesis were detected via Dumas combustion and the oxygen flask method but play no fundamental role in the mineral structure. Around 23% of the sample composition (63% of the oxygen) was inferred from the inevitable formation of iron oxides during pyrolysis.

Element	Relative abundance
Fe	1(±0.012)
O	2.4(±0.056)
H	1.59(±0.022)
Cl	0.03(±0.001)
C	0.04(±0.001)

(ICP-OES JY 2000, Horiba Jobin Yvon Ltd., Stanmore, UK). CHN and O analysis were carried out by Elemental Microanalysis Ltd (Okehampton, Devon). CHN quantification was achieved via Dumas Combustion and GC-TC (EA1110, CE Instruments, Wigan, UK), whilst oxygen content was determined via Unterzaucher Pyrolysis and GC-TC (NA2000, Fisons). Chlorine quantification was carried out via the oxygen flask method with a mercuric nitrate titrant solution and diphenylcarbazone indicator; Table II provides details.

D. Neutron diffraction

Neutron diffraction experiments were carried out with the Near and InterMediate Range Order Diffractometer (NIMROD) instrument at the UK's pulsed neutron and muon source, ISIS (Harwell-Oxford). This instrument is able to simultaneously access length scales from <1 Å to >300 Å, thus providing robust bond-length information at the required length scales. Moreover, as noted above, the study was undertaken with material dried at just 40 °C thereby maintaining its natural 2L-Fh structure. A null scattering vacuum-sealed $Ti_{0.676}Zr_{0.324}$ alloy sample holder, sealed against the instrument vacuum using PTFE o-rings, was used to collect scattering data at 293 K for 123 minutes. Collected data were corrected for background, multiple scattering and absorption, and normalized to a vanadium calibration standard using GUDRUNN [25]. Neutron wavelengths from 0.05 to 14 Å over a momentum transfer range of $0.02\text{Å}^{-1} \leqslant Q \leqslant 50\text{Å}^{-1}$ were used to generate the interference differential scattering cross section, which was Fourier transformed to the Pair Distribution Function (PDF) [26].

Full and partial pair distribution functions (PDFs) were calculated for modelled structures and previously published models, using PDFGUI [27]. For the purposes of generating the PDFs, the models were constructed as laid out in the appropriate, previously published work [10,15]. For the three-phase model, this required the production of a composite PDF, created from the appropriate proportions of the three structures proposed in the model: namely, defective, defect-free, and hematite.

E. Computational modelling

First-principles density functional theory (DFT) calculations were carried out using the plane-wave simulation code, CASTEP [28]. A kinetic energy cut-off, determined through convergence testing, of 700 eV was employed along with a Monkhorst Pack $3 \times 3 \times 3$ k-point grid for sampling of the Brillouin zone [29], giving a maximum k-point separation of 0.05 2π/A. Convergence tolerances for energy change, maximum displacement, maximum force, and maximum stress were set at 1×10^{-5} eV atom^{-1},0.001 Å,0.03 eV Å^{-1}, and 0.05 GPa, respectively. Ultrasoft pseudopotentials (BIOVIA library) were employed [30] along with the local spin-density approximation (LSDA) exchange-correlation functional [31]. The strongly correlated $3d$ iron electrons were corrected with the Hubbard U formulation at 4 eV [32]. The electronic ground state was found using the spin-polarized ensemble density functional theory method [33]. The spin states, corresponding to the ferromagnetic ground state, were the same as those previously calculated by Pinney *et al.* [34].

The starting structure for the single-phase model, which is isostructural with akdalaite, has a $P6_3mc$ space group and lattice parameters of $a = b = 5.95$ Å and $c = 9.06$ Å [15]. However, the space group was altered to P1 for the DFT simulation, to allow complete freedom of all parameters, thus removing the $a = b$ constraint. It should be noted, however, that notwithstanding this relaxation in the crystal symmetry, the structure did retain $a = b$ lattice parameters at the completion of the geometry optimization.

III. RESULTS AND DISCUSSION

A. Ferrihydrite sample analysis

XRD analysis of synthetic ferrihydrite was undertaken to provide mineral phase confirmation. This yielded two diffuse maxima, which was both typical of and consistent with reference peaks for 2L Fh [Fig. 1(a)].

Further to this phase confirmation, we used the NIMROD neutron diffraction data to interrogate both particle size and shape. Fitting a two-sphere correlation model to the low-Q region of the NIMROD data ($0.02 < Q < 1.0$) [Fig. 1(b)] yielded positive results, suggesting a good fit with a spherical particle shape. A nanocrystallite size distribution was also produced with a mean particle diameter of 3.4 nm ±0.5 Å [Fig. 1(c)], which falls within the expected size range (2–5 nm diameter) of two-line Fh, as previously determined from high-resolution TEM [8].

Elemental analysis (Table II) suggests a formula of $5Fe_2O_3 \cdot 8H_2O$, in line with bulk Fh [24] or a heavily hydrated form of Fh as proposed by Michel *et al.* [15], namely, $Fe_{10}O_{14}(OH)_2 \cdot 7H_2O$. Hiemstra *et al.* determined that Fh particle hydration inversely correlates with particle diameter, decreasing from a water content of ∼19% for 2 nm particles, to ∼14% for 3 nm particles and below 10% for 8 nm diameter particles [35,36]. Our analysis indicates that the water content of this synthetic Fh (15.3%) is slightly higher than the reported values for 3-nm Fh particles, attributable to the retention of physisorbed surface water, a consequence of the low drying temperature (40 °C) used to preserve local Fh structure [18]. It is worth noting that according to the calculations of Hiemstra *et al.*, a 2.5 nm

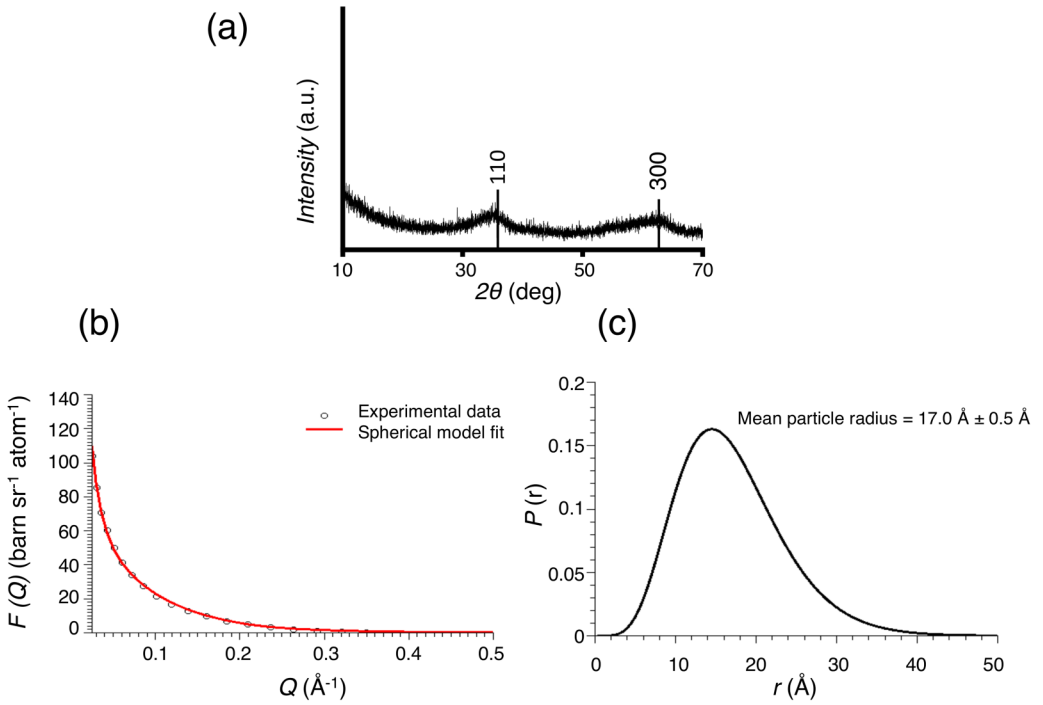

FIG. 1. (a) Ferrihydrite x-ray powder diffraction pattern, overlaid with reflections for two-line Fh. (b) Fitting of the NIMROD experimental data to a simple spherical model. (c) Distribution of nanoparticle sizes within the sample as determined by NIMROD: peak radius is 17 Å.

particle could be classed almost entirely as "surface" with at least 67% of the tetrahedral Fe being directly bound to a surface moiety and the surface "felt" by most of the other ions [35]. This is indicative of the amorphous nature of the mineral, and hence its lack of long-range order. Indeed, a recent study using Mössbauer spectroscopy showed that atomic vacancies and structural disorder are most prevalent at the particle surface, which may be a reason why smaller particles appear to have the greatest amount of disorder [37].

B. Pair distribution function analysis

To investigate the structural detail further, we employed pair distribution function (PDF) analysis to calculate the distances between ion-ion pairs. The normalized all-ion PDF was constructed directly from the neutron diffraction data (Fig. 2).

Despite drying, the large trough at 0.95 Å indicates that a substantial amount of hydrogen remains in the material. Due to hydrogen's negative scattering length, hydrogen associated peaks, such as O-H, have negative intensities or dampened positive signals. This distance (0.95 Å) is slightly shorter than the O-H distance in water (0.98 Å), which points towards the hydrogen being found in OH groups, principally on the surface, rather than as structural water. In a previous neutron diffraction study on a heated deuterated ferrihydrite sample, this trough can be seen as a positive peak at approximately the same r value [9].

Figure 3 shows the same all-ion PDF of Fig. 2, together with the PDFs from the two most accepted ferrihydrite structures published in the literature: the original (2007) single-phase [15] and three-phase models [10]. The latter model was constructed in the 6:3:1 proportion stated in the original paper, composed of a defect-free phase, a defective phase and nanohematite, respectively [10]. The inset in Fig. 3 shows the detail of the first positive peak (A), which is indicative of the Fe-O distance (Fig. 3). Clearly, this peak is modelled more accurately by the single-phase model.

With reference to the experimental PDF in Fig. 3, it is worth noting the large impact of the surface-bound hydrogen, which, due to its negative scattering intensity, reduces the peak heights, dampening the positive signal. This accounts for the smaller peak heights in the experimental data. As already explained above, this surface-bound hydrogen, which was not removed from the particles' surfaces in a high-temperature drying step, marks one of the most important differences between the hydrated synthetic mineral and the structural

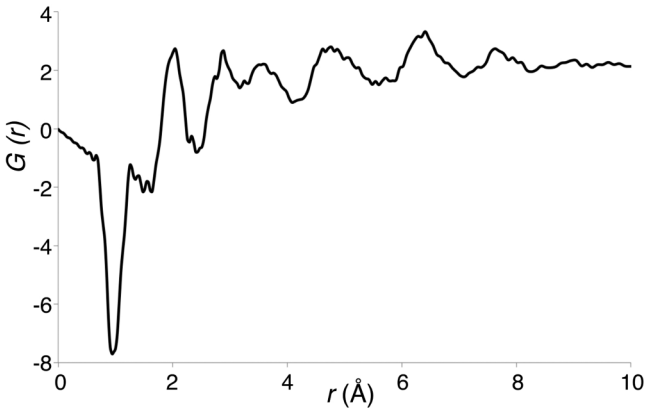

FIG. 2. Neutron-diffraction generated all-ion PDF for fully hydrated synthesized two-line ferrihydrite. The large negative trough at 0.95 Å is accounted for by an O-H correlation.

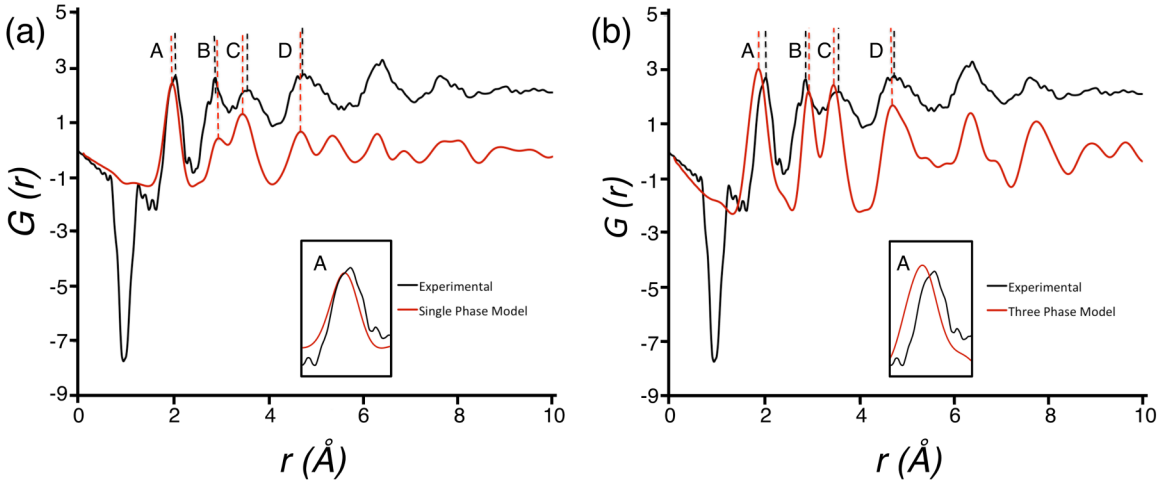

FIG. 3. Neutron-diffraction generated all-ion PDF for synthetic two-line ferrihydrite (black) compared with, in red, (a) the all-ion PDF of the original single-phase two-line model [15] and (b) the three-phase model [10]. The fully crystalline model PDFs have been attenuated using an exponential function, $G(r) = G(r)_0\, e^{-0.234r}$, to mimic the decay signal at larger distances (r values) that would be found in a nanoparticulate sample. This exponential was intended not as a fit to the experimental data, but simply to remove the long-range crystallinity inherent in the modelled PDFs. The insets show peak A, which represents the first Fe-O bond length, in detail.

models. Equally, the large negative peak in the experimental PDF at 0.95 Å, which represents surface bound OH, is not observed in the model PDF as this is calculated from a bulk rather than surface structure.

As shown in Fig. 4(c), peaks a, d, and f [as labelled in Fig. 4(a)] are almost entirely identifiable as the distances between Fe and O ions. Peak c is strongly accounting for both the Fe-Fe [Fig. 4(b)] and Fe-O [Fig. 4(c)] distances. However, other peaks, particularly b and e, represent a number of different ion-ion pairs. Thus, with reference to Fig. 2, the average Fe-O bond length in the synthesized Fh is 2.04 Å, with further Fe-O distances of 4.77 and 6.42 Å. Other peaks were not securely assigned to particular ion pairs, due to overlap in signal.

The experimental Fe-O bond length (2.04 Å) is closer to the single-phase model (2.00 Å, [15]) than the three-phase model (1.90 Å, Ref. [10]), although it should be noted that this single-phase model includes heavily distorted Fe tetrahedra that have one shorter Fe-O bond, in defiance of Pauling's second law. The three-phase model Fe-O bond length, obtained from the composite PDF, fits poorly to the new data and to other reported Fe-O distance data (1.97 A) obtained via x-ray

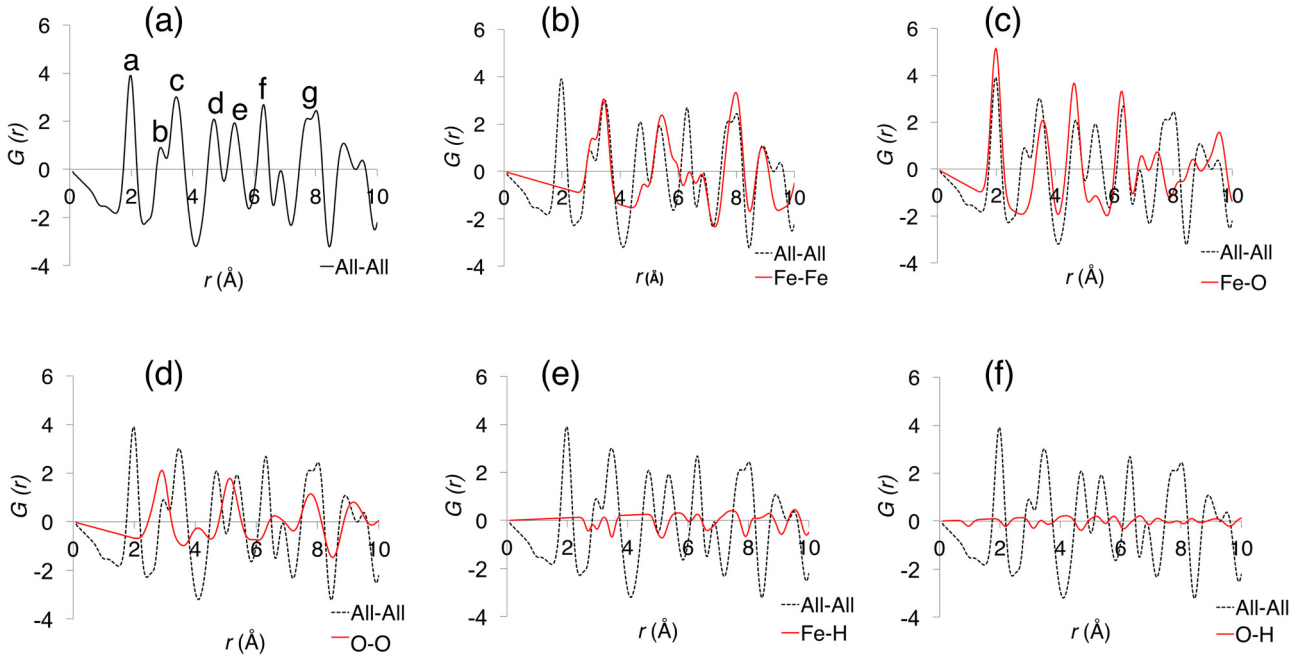

FIG. 4. The split all-ion PDF of the single-phase two-line model [15]. The all-ion PDF is shown in black in each frame and the individual PDFs are shown in red: (a) all-ion, (b) Fe-Fe, (c) Fe-O, (d) O-O, (e) Fe-H, and (f) O-H. The H-H PDF only has a very minor effect on the all-ion PDF and has, for clarity, not been shown.

TABLE III. Lattice parameters of the new DFT-optimized ferrihydrite model, compared to the two-line single-phase model of Michel *et al.* [15]. The percent values in brackets, are the difference between the given DFT model and that of Michel *et al.* [15].

Parameter	Optimized two-line DFT	Single-phase two-line (*18*)
a (Å)	5.84(−1.9%)	5.96
b (Å)	5.84(−1.9%)	5.96
c (Å)	9.15(+2.1%)	8.97
Volume (Å^3)	270.66(−1.8%)	275.60

absorption fine structure (EXAFS) spectroscopy [18]. Even if the proportions of the defective and defect-free phases are varied for this latter model, it is only when the model reaches its defect-free maximum that the Fe-O peak, at around 1.93 Å, approaches the lowest point of the experimental data peak. Doing this, however, eliminates the amorphous character of the mineral (which was effectively modelled by the defective phase), making the structure altogether unrealistic.

We next sort to address whether the single-phase model could be refined to better fit the experimental data and to address some of the inconsistencies previously noted and discussed above. In particular, the tetrahedrally bonded Fe atoms have one short Fe-O bond (as low as 1.79 Å in the six-line model), making the tetrahedra heavily asymmetric [20,21,34]. Furthermore, the octahedral and tetrahedral Fe-O bond lengths are approximately equal and hence the space occupied by these two environments is almost the same, which is dubious [21]. Notwithstanding, as a starting point, we took this best current estimate of the two-line single-phase structure [15] and, using DFT, performed a geometry optimization to see if improvements could be made that match the experimental NIMROD data (previous DFT optimization has been reported but using the six-line single-phase structure as the starting position [34]). The lattice parameters for the resulting model are presented in Table III. Although we did not constrain the a and b parameters, unlike in the work with the refined six-line model [34], they did, nevertheless, remain equal.

In the refined structure, the a and b parameters are reduced compared to the prior state-of-the-art 2L-Fh model (Table III), while the c parameter is increased; an even greater increase in the c parameter is also observed in the previous six-line Fh DFT refinement. This was explained by the authors as an illustration of the inherent crystallinity of their model as compared to the experimentally derived model [15], an argument that is equally well applied to our DFT results. Indeed, our c-parameter is just 0.3% longer than that of the experimentally derived value, which comes from the most crystalline of the samples [15].

Further to the results above, geometry optimizations of all three single-phase structures (two-, three-, and six-line ferrihydrite) and the optimized six-line DFT structure have been carried out. All these optimized structures relaxed to the same structure (within two decimal places) as the model described by the parameters in Table III. Complete structural parameters are presented in Table IV and in the cif file included in Ref. [38].

Although not a defining feature of the ferrihydrite phase compared to other iron oxides and oxohydroxides, it is worth

TABLE IV. Complete structural parameters for the new DFT-optimized ferrihydrite model. The structure was optimized with a $P1$ space group to allow the structure to relax with complete freedom. On completion, the space group was recalculated and found to be $P6_3mc$ with a maximum deviation from symmetry of 0.51×10^{-14} Å.

Lattice Parameters

a (Å)	b (Å)	c (Å)	α(°)	b(°)	γ(°)
5.843	5.843	9.154	90.000	90.000	120.000

Space Group: $P6_3mc$

Fractional Coordinates

Atom	x	y	z
H1	−0.000003	−0.000003	0.405147
H2	−0.000003	−0.000003	0.905147
O1	−0.000003	−0.000003	0.014398
O2	−0.000003	−0.000003	0.514398
O3	0.333330	0.666663	0.754598
O4	0.666663	0.333330	0.254598
O5	0.166322	0.833672	0.244881
O6	0.166322	0.332647	0.244881
O7	0.667346	0.833672	0.244881
O8	0.833672	0.166322	0.744881
O9	0.833672	0.667346	0.744881
O10	0.332647	0.166322	0.744881
O11	0.514510	0.485483	0.005146
O12	0.514510	0.029024	0.005146
O13	0.970969	0.485483	0.005146
O14	0.485483	0.514510	0.505146
O15	0.485483	0.970969	0.505146
O16	0.029024	0.514510	0.505146
Fe1	0.166395	0.833599	0.638163
Fe2	0.166395	0.332793	0.638163
Fe3	0.667200	0.833599	0.638163
Fe4	0.833599	0.166395	0.138163
Fe5	0.833599	0.667200	0.138163
Fe6	0.332793	0.166395	0.138163
Fe7	0.333330	0.666663	0.341255
Fe8	0.666663	0.333330	0.841255
Fe9	0.333330	0.666663	0.958231
Fe10	0.666663	0.333330	0.458231

noting that the Fe-Fe bond lengths obtained from the DFT optimization, at 2.92 and 3.20−3.54 Å, are entirely in keeping with a structure of this chemical composition. For comparison, the neutron diffraction data predicts these peaks at 2.89 and 3.41–3.58 Å, although it is recognized that these peaks also contain some contributions from other ion pairs (see Fig. 4) and hence do not correspond precisely to the Fe-Fe distances. Fe-O bond lengths in the DFT model were also analysed and bond populations calculated using the Mulliken formalism to define electron distribution between ions [39]. Octahedral Fe sites were little changed, at 2.00 Å, compared to those of the original single-phase model, but significant differences emerged for the tetrahedral Fe sites. Table V shows the refined bond lengths and bond populations for tetrahedral Fe.

The DFT refinements led to increased bond populations and shortened tetrahedral Fe-O bond lengths, resolving several

TABLE V. The calculated bond populations and bond lengths of the Fe-O bonds for the tetrahedrally coordinated Fe ions.

Previous single-phase model		DFT-optimized model	
Fe-O bond population ($\|e\|$)	Fe-O bond length (Å)	Fe-O bond population ($\|e\|$)	Fe-O bond length (Å)
0.38	1.959	0.42	1.864
0.45	2.019	0.49	1.883
0.45	2.019	0.49	1.883
0.45	2.019	0.49	1.883

criticisms of the previous single-phase model. Crucially, tetrahedral Fe-O bond lengths are contracted to an energetically more favorable 1.88 Å, reflecting the increased electrostatic bond strength associated with lower coordination environments. Whilst a previous DFT refinement [34] partially addressed this failing of the original model, their tetrahedral Fe-O bond length (1.92 Å) remained outside the plausible range for Fe^{3+} tetrahedral sites [21,40]. Furthermore, tetrahedral distortion has been virtually eliminated and site volume was reduced by 17%, as shown in Fig. 5(a).

While in the previous single-phase structure both the tetrahedral and octahedral Fe ions have average Fe-O bond lengths of 2.00 Å [15], in our new DFT optimization, Table IV, the octahedral Fe-O bonds retain a 2.00 Å average but the tetrahedral average is now 1.88 Å. Crucially, plausible tetrahedral Fe-O bond lengths were achieved and these were in line with expectations for such an Fe site based upon published comparisons of inorganic crystal structures [21,41]. This refinement therefore remains consistent with our experimental data (average Fe-O bond length of 2.04 Å) but significantly reduces the tetrahedral site volume. Furthermore, the eccentricity of this tetrahedral volume has been significantly reduced with just 1% (rather than 3% [15]) difference between the "short" bond and the other bonds of the tetrahedra. The previous DFT six-line refinement also reduced the tetrahedral Fe-O bond length but to a lesser extent, to 1.92 Å [34], and still above the range cited by other authors as acceptable [21].

While these refinements resolve the previous chemical inconsistencies, it is clearly important that the new structure is able to reproduce XRD features of the original model, being consistent with experimental XRD data. Figure 5(b) shows simulated XRD patterns for both the original single-phase two-line structure [15] and the new refinement; it is clear that this new refinement retains good fit with the original data, and the two major peaks at around 35° and 63° are consistent with those in our own heavily broadened 2L-Fh XRD pattern, shown in Fig. 1(a).

IV. CONCLUSIONS

The NIMROD instrument at ISIS was able to produce an accurate diffraction pattern with 2L-Fh material dried at ambient temperatures, which, for the first time, obviated dehydration and removed the possibility of phase transformation through heating steps that were necessary for analysis with prior instrumentation. Naturally, hydrated nanoparticulate two-line ferrihydrite has an extremely large surface: volume ratio and has a surface that is heavily populated with OH groups, accounting for more than 15% of the particle weight. Our results are best explained by a single-phase model that allows for tetrahedrally coordinated iron, in contrast to the octahedral-only three-phase model, which is incompatible with the primary Fe-O bond length and amorphous characteristics of the mineral.

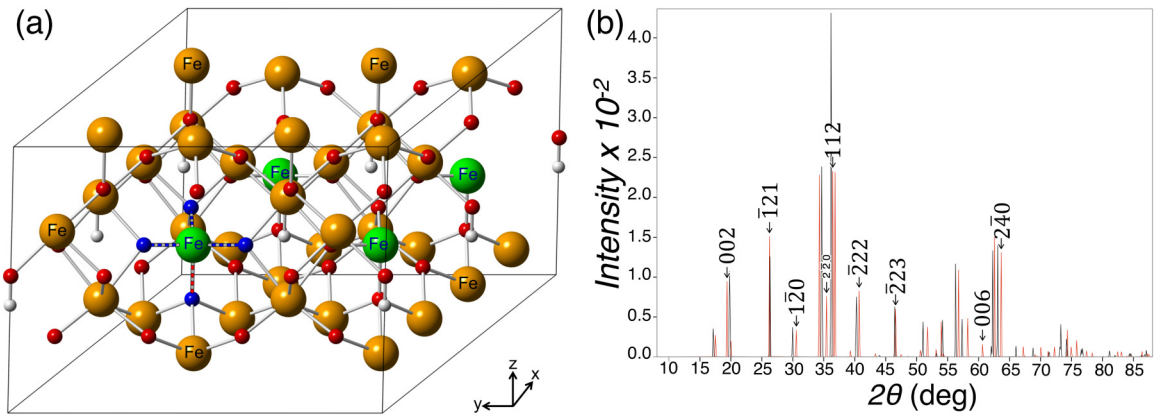

FIG. 5. (a) DFT-optimized single-phase 2L ferrihydrite. The tetrahedral Fe ions are shown in green and the octahedral Fe ions in orange. In this new structure, the tetrahedral Fe site is reduced by 17% compared to the original single-phase model [15]. The new Fe_{tet}-O bond lengths are 1.883 (blue-banded) and 1.864 Å (red-banded). The directly bonded oxygen atoms for the example tetrahedral sites are shown in dark blue, all other oxygen ions are shown in red and hydrogen in white. For clarity, some ions have been removed from the illustration to make the example tetrahedral sites completely visible, and all surfaces have periodic boundary conditions. (b) Simulated XRD patterns for the previous (black) and refined (red) single-phase models.

Crucially, following DFT optimization of the previous state-of-the-art single-phase model [15], we can now propose a structure that has lattice parameters fully consistent with experimental data and with tetrahedral Fe sites that do not conflict with basic principles of coordination chemistry. We present a model that has a refined and yet simplified crystallography and is consistent with both the experimental XRD diffraction pattern and the neutron PDF of naturally-hydrated ferrihydrite.

ACKNOWLEDGMENTS

The modelling work was performed using the Darwin Supercomputer of the University of Cambridge High Performance Computing Service (http://www.hpc.cam.ac.uk/), provided by Dell Inc. using Strategic Research Infrastructure Funding from the Higher Education Funding Council for England and funding from the Science and Technology Facilities Council. HC, NF, and JJP would like to thank the UK Medical Research Council (Grant No. MC_U105960399) for their support. Work was carried out on the ISIS Nimrod instrument over three days under STFC experiment RB1400012. The authors would like to thank Lesley Neve at the School of Earth and Environment, University of Leeds, for carrying out the XRD measurements, Alan Soper (Rutherford Appleton Laboratory) for help with analyzing the particle shape and Andy Brown at the University of Leeds for reviewing the final draft.

H.F.C, W.T., D.T.B., and N.F. all contributed to running the neutron diffraction experiments at ISIS, H.F.C and P.J.H. carried out the modelling component of the project. All authors were involved in discussions as to the objectives and interpretation of the final results. The manuscript was written by H.F.C. with contributions from all authors, and editing from D.T.B and J.J.P.

[1] T. A. Jackson and W. D. Keller, Am. J. Sci. **269**, 446 (1970).
[2] A. C. Birnie and E. Paterson, Geoderma. **50**, 219 (1991).
[3] J. L. Jambor and J. E. Dutrizac, Chem. Rev. **98**, 2549 (1998).
[4] P. M. Harrison, Fa. Fischbac, T.G. Hoy, and G. H. Haggis, Nature (London) **216**, 1188 (1967).
[5] Y. Wu, W. Zhang, W. Yu, H. Liu, R. Chen, and Y. Wei, Front. Environ. Sci. Eng. **9**, 411 (2015).
[6] S. Neiser, F. Rentsch, U. Dippon, A. Kappler, P. G. Weidler, J. Göttlicher, R. Steininger, M. Wilhelm, M. Braitsch, F. Funk, E. Philipp, and S. Burckhardt, BioMetals. **28**, 615 (2015).
[7] O. Sadeghi, L. N. Zakharov, and M. Nyman, Science **347**, 1359 (2015).
[8] H. Liu, X. Li, Y. Wang, X. Yang, Z. Zhen, R. Chen, D. Houb and Y. Wei, RSC Adv. **4**, 11451 (2014).
[9] R. Harrington, D. B. Hausner, W. Xu, N. Bhandari, F. M. Michel, G. E. Brown, Jr., D. R. Strongin, and J. B. Parise, Environ. Sci. Tech. **45**, 9883 (2011).
[10] V. A. Drits, B. A. Sakharov, A. L. Salyn, and A. Manceau, Clay Min. **28**, 185 (1993).
[11] A. Manceau and W. P. Gates, Clays. Clay. Min. **45**, 448 (1997).
[12] S. M. Heald, E. A. Stern, B. Bunker, E. M. Holt, and S. L. Holt, J. Amer. Chem. Soc. **101**, 67 (1979).
[13] R. A. Eggleton, and R. W. Fitzpatrick, Clays. Clay. Min. **36**, 111 (1988).
[14] G. Vaughan, R. Brydson, and A. Brown, J. Phys.: Conf. Ser. **371**, 012079 (2012).
[15] F. M. Michel, L. Ehm, S. M. Antao, P. L. Lee, P. J. Chupas, G. Liu, D. R. Strongin, M. A. A. Schoonen, B. L. Phillips, and J. B. Parise, Science **316**, 1726 (2007).
[16] F. M. Michel, V. Barrón, J. Torrent, M. P. Morales, C. J. Serna, J-F. Boily, Q. Liu, A. Ambrosini, A. C. Cismasu, and G. E. Brown, Jr., Proc. Natl. Acad. Sci. USA **107**, 2787 (2010).
[17] J. Zhao, F. E. Huggins, Z. Feng, and G. P. Huffman, Clays. Clay. Min. **42**, 737 (1994).
[18] F. Malliot, G. Morin, Y. Wang, D. Bonnin, P. Ildefonse, C. Chaneac, and G. Calas, Geochim. Cosmochim. Acta. **75**, 2708 (2011).
[19] D. G. Rancourt and J.-F. Meunier, Am. Min. **93**, 1412 (2008).
[20] A. Manceau, S. Skanthakumar, and L. Soderholm, Am. Min. **99**, 102 (2014).
[21] A. Manceau, Clay Min. **44**, 19 (2009).
[22] A. Manceau, Am. Min. **96**, 521 (2011).
[23] K. M. Towe and W. F. Bradley, J. Coll. Inter. Sci. **24**, 384 (1967).
[24] E. Jansen, A. Kyek, W. Schäfer, and U. Schwertmann, Appl. Phys. A **74**, S1004 (2002).
[25] A. K. Soper, Rutherford Appleton Laboratory Technical Report, RAL-TR-2011-013 (2011).
[26] A. K. Soper and E. R. Barney, J. Appl. Cryst. **45**, 1314 (2012).
[27] C. L. Farrow, P. Juhás, J. W. Liu, D. Bryndin, E. S. Božin, J. Bloch, Th. Proffen, and S. J. L Billinge, J. Phys.: Condens. Matter. **19**, 335219 (2007).
[28] S. J. Clark, M. D. Segall, C. J. Pickard, P. J. Hasnip, M. I. J. Probert, K. Refson, and M. C. Payne, Z. Kristallogr. **220**, 567 (2005).
[29] H. J. Monkhorst and J. D. Pack, Phys. Rev. B **13**, 5188 (1976).
[30] D. Vanderbilt, Phys. Rev. B **41**, 7892 (1990).
[31] M. C. Payne, T. A. Arias, and J. D. Joannopoulos, Rev. Mod. Phys. **64**, 1045 (1992).
[32] M. Cococcioni and S. de Gironcoli, Phys. Rev. B **71**, 035105 (2005).
[33] N. Marzari, D. Vanderbilt, and M. C. Payne, Phys. Rev. Lett. **79**, 1337 (1997).
[34] N. Pinney, J. D. Kubicki, D. S. Middlemiss, C. P. Grey, and D. Morgan, Chem. Mater. **21**, 5727 (2009).
[35] T. Hiemstra, Geochim. Cosmochim. Acta. **105**, 316 (2013).
[36] W. Xu, D. B. Hausner, R. Harrington, P. L. Lee, D. R. Strongin, and J. B. Parise, Am. Min. **96**, 513 (2011).
[37] X. Wang, M. Zhu, L. K. Koopal, W. Li, W. Xu, F. Liu, J. Zhang, Q. Liu, X. Feng, and D. L. Sparks, Environ. Sci.: Nano. **3**, 190 (2016).
[38] See Supplemental Material at http://link.aps.org/supplemental/10.1103/PhysRevMaterials.1.036002 for the new ferrihydrite structure file.
[39] M. D. Segall, R. Shah, C. J. Pickard, and M. C. Payne, Phy. Rev. B **54**, 16317 (1996).
[40] A. N. Shmakov, G. N. Kryukova, S. V. Tsybulya, A. L. Chuvilin, and L. P. Solovyeva, J. Appl. Cryst. **28**, 141 (1995).
[41] I. D. Brown and D. Altermatt, Acta. Cryst. B **41**, 244 (1985).